SSC20-WP2-17

Water Vapor Independent Satellite Propulsion System (WISP) for Nanosatellite Orbit Maintenance

Ian A. Hardy, Jin S. Kang, Jeffery T. King
United States Naval Academy
590 Holloway Rd., MS 11B, Annapolis, MD 21402
kang@usna.edu

ABSTRACT

While nanosatellites have been widely implemented for scientific applications, power constraints, large free-space path losses, and system complexity prevent many researchers from fielding novel sensing hardware. Additionally, dead-on-arrival missions contribute to the growing volume of orbital debris. Access to lower orbits would decrease downlink losses, improve optical sensor performance, and ensure natural de-orbit for inoperable payloads. Conventional satellite propulsion technologies are capable of providing thrust required to maintain a low orbit, but increase system complexity and draw power away from the sensors. The United States Naval Academy has developed the Water Vapor Independent Satellite Propulsion system (WISP) to maintain orbits as low as 250km without drawing electrical power during steady state operation. This system utilizes an aqueous methyl alcohol propellant that passively evaporates across a phase separation boundary prior to exiting through a nozzle. Since this process occurs passively based on propellant evaporation properties and expansion chamber conditions, no electrical power is required during steady state operation. Theoretical calculations show that this system of 1U volume (10 x 10 x 10 cm) is capable of providing sufficient thrust to maintain orbit for approximately 30 days.

INTRODUCTION

Nanosatellites offer an effective solution to laboratories, commercial entities, and academic institutions that require access to low earth orbits for data collection. These satellites are increasingly used in lieu of traditional, multi-instrument platforms due to their low-cost, abundance of rideshare opportunities, and their implementation of commercial-off-the-shelf components. However, many CubeSats arrive on orbit in an inoperable condition and contribute to the growing problem of orbital debris. Even for those payloads that function properly in orbit, power constraints and large free-space path losses limit what sensing hardware can be implemented. If a means of maintaining orbit at low altitudes without drawing significant electrical power were available, new sensing technologies could be more easily fielded with improved performance while ensuring de-orbit after mission conclusion.

CubeSat data downlink capability is frequently limited by small, low-power hardware solutions resulting from form factor and power availability constraints. These limitations could be partially mitigated by reducing free-space path losses by deploying at a lower orbital altitude. Deploying at such an altitude would also increase the effectiveness of optical sensing hardware by decreasing distance between sensors and points of interest. With smaller losses and lower design focal lengths, image data could be collected at higher resolution while implementing smaller apertures. Using lower orbits would improve data collection and reduce the amount of power diverted to non-sensor hardware.

While low orbits are favorable in terms of data collection and communications signal gains, increasing drag forces acting on spacecraft at these altitudes would cause de-orbit within a few days of deployment. Implementing a propulsion system could counteract drag to maintain orbit, but would do so at a substantial power cost. Satellite propulsion systems also add mechanical complexity and frequently require more complicated integration procedures due to the presence of compressed gas or other propellant. Complications in systems and process engineering and power limitations render conventional propulsion systems inaccessible to most nanosatellite applications. Additionally, propellant types may also restrict the ability to launch the satellites on all launch platforms or with many rideshare opportunities.

In order to provide sufficient thrust to counteract drag at 250km or higher orbits, the United States Naval Academy has designed the Water Vapor Independent Satellite Propulsion system (WISP). This cold gas thruster draws no power during steady state operation as liquid propellant passively evaporates across a phase separation boundary and is accelerated through a nozzle. Constant inlet pressure for the thruster is maintained by propellant evaporation until the reservoir is depleted, at which point the satellite will de-orbit quickly due to the

air drag. Should a fault occur that renders the satellite dead-on-arrival, the propulsion system would not actuate, causing the satellite to naturally de-orbit within a few days due to its low altitude. This capability is contained within a 1U bolt-on architecture that allows for streamlined integration and use by members of the scientific community who lack dedicated satellite build capability.

Designed to provide thrust for nanosatellites meeting the CubeSat standard, WISP offers researchers the opportunity to collect data from the space environment without needing to design and integrate a custom bus, power management system, or communications hardware. Instead, scientific instruments can be installed directly into a universal bus system providing propulsion and attitude stabilization until natural deorbit at the end of the mission. This architecture would allow much greater numbers of researchers and institutions to contribute earth science data without adding to the volume of debris currently in orbit.

SYSTEM ARCHITECTURE / CONOPS

The Water Vapor Independent Satellite Propulsion system (WISP) is self-contained and designed for implementation in a 3U CubeSat form factor. The system is composed of five main components: a liquid propellant reservoir, a passive phase separator, a 165mL gas expansion chamber, a converging-diverging micronozzle, and four deployable attitude stabilization surfaces. These components are depicted as part of a conceptual rendering below in Figure 1.

WISP is mounted within 1U on the "bottom" of a CubeSat payload of up to 2U in total volume. The above figure demonstrates WISP's modular design and in-line assembly method which enable rapid implementation by laboratories lacking dedicated in-house satellite build capability.

The propellant reservoir ("1" in Figure 1) is capable of carrying up to 835mL of propellant at 1ATM. The 135mL expansion chamber ("3" in Figure 1) allows evaporating propellant to expand and maintain inlet pressure for the nozzle assembly mounted on the outboard face of the chamber. The reservoir and expansion chamber interface only through means of a passive phase separation plane located along their adjoining surfaces. This phase separator exploits propellant surface tension properties to selectively retain liquid while allowing vapor to flow into the chamber. For the purpose of this rendering, nozzle diameter and phase separator pore sizes are greatly exaggerated. Actual attitude stabilizers would be offset from the chassis by at least 30cm, but are shown in a closer orientation for ease of visualization.

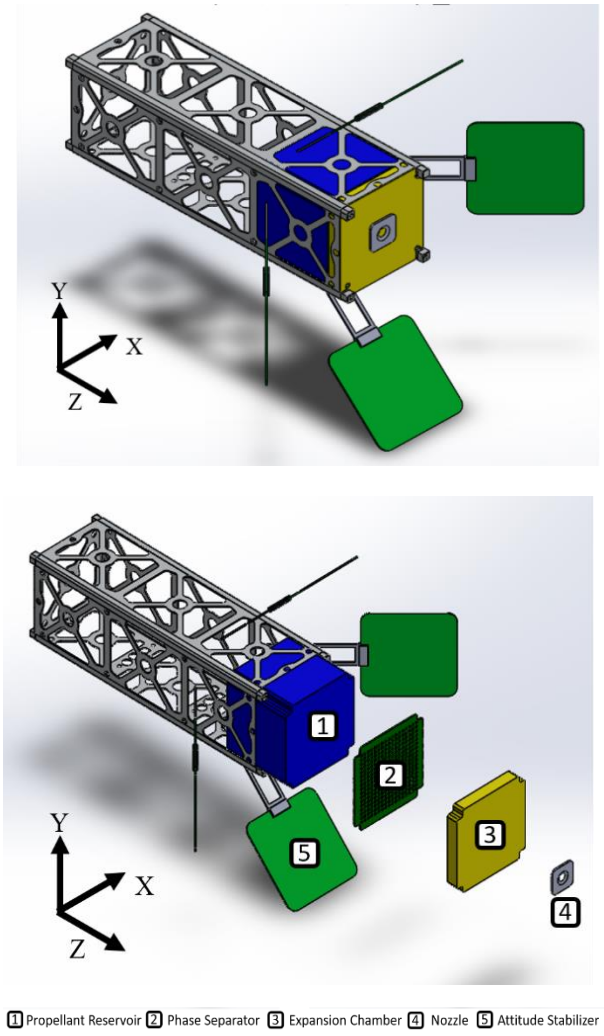

Figure 1. Isometric concept render of WISP within 3U CubeSat chassis

The propellant reservoir and expansion chamber occupy the majority of WISP's total volume and are bolted to the satellite chassis. The phase separator ("2" in Figure 1) is mounted between the reservoir and chamber by bolting tabs located on the outside edge of the separator to the propellant reservoir body. The combined reservoir-separator-chamber assembly is sealed together with epoxy. Lastly, the nozzle plate is fastened to the chamber and sealed with epoxy. Detailed specifications for fastening techniques, the nozzle valve actuation system, and pressure testing are not included in this study.

Once the exit plane of the nozzle is opened after reaching a stable on-orbit attitude, gas present in the expansion chamber will evacuate through the nozzle. As this gas evacuates, the pressure within the chamber will decrease, creating a pressure difference between reservoir and chamber and inducing flow of vapors generated at each separator pore.

Attitude stability is provided by atmospheric drag acting on attitude stabilizer surfaces. Since these surfaces deploy at a 135° angle relative to the surface of the satellite, any variation in attitude will alter the fraction of each surface that is normal to the direction of motion. This arrangement minimizes drag forces when WISP's z-axis is aligned with the direction of motion, providing a natural method of stabilizing satellite attitude. Previous design studies indicate that these attitude stabilizers would provide enough restoring moment to limit off-axis deviation between the Z-axis and direction of motion to roughly 20° [1].

WISP streamlines the integration, testing, and launch process for nanosatellites by providing propulsion and attitude stabilization capability for CubeSat form factor missions. Utilizing an independent system architecture that does not interface with sensing hardware, WISP can be installed in a fraction of the time usually required to assemble other propulsion and attitude stabilizer systems. This allows WISP to be installed in a short period of period of time with minimal manpower. A sample concept of operations is depicted below in Figure 2.

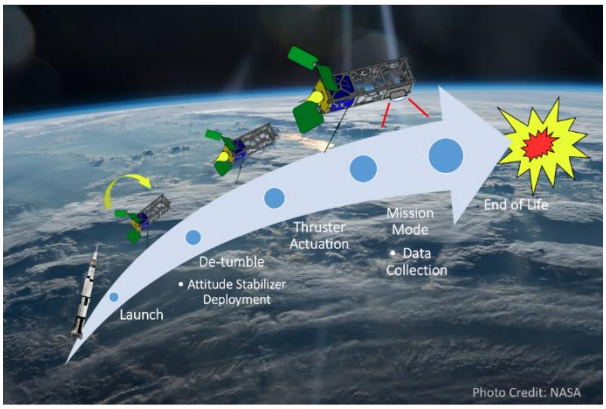

Figure 2. Sample WISP concept of operations

Prior to integration, the propellant reservoir will be filled and mated with the phase separator, expansion chamber, and nozzle assembly. The combined assembly may either be immediately mounted to the satellite chassis or stored until client payload is ready for integration. Propellant is shelf-stable and can be stored at 1ATM indefinitely.

During the integration process, attitude stabilizers can be mounted to either the satellite chassis or the exterior of the propellant reservoir. Stabilizers will then be preloaded for deployment and stowed. Once on orbit, these surfaces will deploy by means of a burn wire, extending out from the satellite body at a 135° angle. Procedures and performance of attitude stabilization hardware are not detailed in this study, but will be published later.

While these components occupy the same chassis as mission hardware, they operate independently of any scientific or communications instrumentation. After reaching the desired orbit, attitude stabilization surfaces will deploy to eliminate tumbling. Once spin rates have been reduced and the satellite has achieved a stable attitude, a valve in the thruster system will open, allowing propellant to flow through the nozzle to maintain orbit until propellant reserves are exhausted.

DESIGN ADVANTAGES

The WISP satellite bus is capable of carrying scientific instrumentation without requiring complex operational planning on the part of the researcher. Passive propulsion and attitude stabilization systems allow earth-observing instruments to maintain pointing for data collection. These systems allow for missions to occur at lower altitudes, improving overall communications and data collection. Standardized system architecture allows researchers unexperienced with space systems engineering to collect data without requiring custom bus design.

By streamlining design and integration processes required to deliver scientific instruments to orbit, WISP will enable researchers to rapidly field new sensing technologies in space. A sample timeline and mission overview are provided in Figure 3. Rapid integration of the modular WISP system allows instruments to be deployed with minimal lead time and collect data for approximately one month.

Since the propulsion system does not consume electrical power during operation, this additional energy can be diverted to larger, more powerful instruments than can traditionally be implemented in satellites of this size. Rudimentary attitude control provided by atmospheric drag stabilization will allow instruments to maintain basic pointing at earth or maintained in the velocity direction. By maintaining a stable attitude, earth-sensing equipment can be utilized to collect much larger volumes of data than is possible through conventional, large-scale satellite missions. One-time thrust actuation reduces potential disturbances during data collection and decreases operational complexity as orbit maintenance is performed constantly rather than by discrete, dedicated maneuvers.

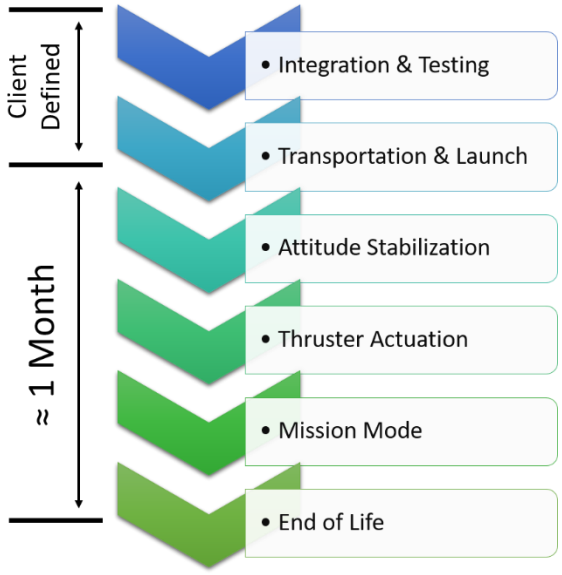

Figure 3. Sample integration and mission timeline

By maximizing propellant volume carried into orbit and optimizing solution properties to increase performance, WISP is designed to provide one month of orbit life at 250km altitude. While this is not suitable for long-duration data collection missions, it is capable of demonstrating new instruments or technology and providing sizable volumes of data to the ground on a modest budge. Furthermore, since WISP is only actuated once, it provides these capabilities without adding to the operational complexity of the mission. By offering these capabilities in a modular form factor, it is easily attached to nearly any payload up to 2U in total volume, and could potentially be implemented on larger systems.

PERFORMANCE ANALYSIS

Design performance depends on the ability to maintain appropriate inlet nozzle inlet pressure throughout the duration of the mission. Chamber pressure is maintained by allowing propellant to evaporate across the phase separator to balance gas evacuation through the nozzle. However, evaporation of solutions containing volatile organic compounds contains many complex, non-ideal processes, including preferential dissipation of more volatile constituents and intermolecular interactions.

Propellant Evaporation Properties

Inlet pressure maintenance relies on ability to predict evaporation behavior exhibited by the propellant. A myriad of factors affects evaporation chemistry, including temperature, viscosity, diffusivity, and density. Additionally, any intermolecular interactions or non-ideal behavior in the propellant solution would alter these properties and the resulting performance. Aqueous methyl alcohol solution used as propellant in this design will exhibit hydrogen bonding between its constituents and preferential evaporation of methyl alcohol. However, without a large volume of experimental data it is difficult to predict the degree to which these non-ideal processes affect system performance.

To simplify performance projection for this propellant, average values for density, viscosity, diffusivity, and vapor pressure were calculated according to the mass percentages and mole fractions of propellant constituents. Polynomial curve fits for density and viscosity were obtained using MATLAB. Since propellant is capable of remaining a liquid between -37°C and 70°C at 1ATM, published properties for methyl alcohol at these temperatures and water stored between 0°C and 70°C were used [2,3,4,5]. The resulting functions for viscosity and density of each constituent are shown below. These functions are listed as functions of temperature below in Table 1.

Using the above data for an operating temperature of 30°C, a weighted average for density and viscosity data were then calculated for a 35% (by weight) aqueous methyl alcohol solution. A propellant specific heats ratio of 1.285 was also determined using this weight percentage and published data [6]. A similar curve fit method was used to determine propellant diffusivity using experimental data for aqueous methyl alcohol

Table 1. Propellant Densities and Viscosities as Functions of Temperature (in Kelvin)

Compound	Density (kg/m^3)	Viscosity (Pa-s)
Water	$-0.004265T^2 + 2.305T + 688.8$ (R^2=0.9992)	$(3.150\times10^{-6})T^2 - (2.127\times10^{-4})T + 0.03635$ (R^2=0.9935)
Methyl Alcohol	1074.3 - 0.9677T (R^2=0.9956)	$(9.251\times10^{-8})T^2 - (6.446\times10^{-5})T + 0.01154$ (R^2=0.999)

reported by Derlacki et al [7] and applied to the mole fraction implemented in WISP propellant. Propellant diffusivity (m^2/s) was then obtained as a function of methyl alcohol mole fraction X as shown below in Equation 1.

$$(3.220\times10^{-9})X^2 - (2.477\times10^{-9})X + 1.501\times10^{-9} \quad (1)$$

Data used for curve fitting were obtained between 0°C and 70°C. Since WISP is designed to operate at 30°C initial temperature for this analysis, these values were deemed appropriate for performance projection at this design point.

Vapor pressure may be found as a function of temperature using the relationship described by the Antoine equation, listed below, and empirical constants for both water and methanol [8].

$$P = 10^{A-\frac{B}{C+T}} \quad (2)$$

where A, B, and C are empirically derived constants. While these projections do not account for non-ideal interactions between propellant constituents, they offer a first approximation to determine the validity of the overall design concept.

Phase Separation

In order to prevent any liquid phase material from entering the expansion chamber, WISP exploits the surface tension properties of the propellant. This separator, composed of a plate containing thousands of nano-scale pores, provides surfaces from which propellant will evaporate according to ambient conditions within the expansion chamber.

The maximum pore radius allowable while retaining liquid is given by the Young-Laplace equation [9], listed below as Equation 3.

$$r = \frac{2\sigma(T)}{\Delta P} \quad (3)$$

Since surface tension strength, σ, decreases with rising temperature, a pore that could retain liquid at maximum operating temperature would also retain liquid at lower temperatures within this range. Since methyl alcohol at standard atmospheric conditions boils at approximately 70°C and maintains lower surface tension than water across WISP operating temperature, separation pore size was calculated using surface tension of pure methyl alcohol at this temperature [10]. Using this method, a 70nm diameter pore was determined to be sufficient to retain propellant in separate phases across its operating range.

Evaporation

Vapor generation at the surface of each pore was calculated using the Van den Bosch equation for pool evaporation, listed here as Equation 4. Convective mass transfer coefficient k_C is determined in Equation 5 using the Sherwood number and diffusivity calculated previously. Additional flow parameters required for this derivation are shown in Equations 6-8 (Bennett 1974) [11].

$$E = k_C \frac{P_V(T)\mathcal{M}}{RT} \quad (4)$$

where E is the evaporative flux per unit area, k_C is the convective mass transfer coefficient (often referred to as mass transfer Nusselt number), P_V represents propellant vapor pressure as a function of temperature, $\mathcal{M}$ is propellant mass, and R and T represent the gas constant and temperature, respectively. The diffusivity of propellant, D, can be calculated using

$$k_C = \frac{D\times Sh}{L} \quad (5)$$

where Sh is the Sherwood Number and L is the pore diameter. For this equation, the Sherwood Number can be obtained from

$$Sh = 0.66Re^{0.5}Sc^{0.33} \quad (6)$$

where Re is the Reynolds Number and Sc is the Schmidt Numbers that can be obtained using

$$Sc = \frac{\mu}{\rho D} \quad (7)$$

$$Re = \frac{\rho V_w L}{\mu} \quad (8)$$

where μ is the viscosity of the fluid, ρ is the fluid density, D is the mass diffusivity, and V_w is the local wind velocity. Using this method, an average propellant evaporative flux of $29.37 mg/m^2s$ was calculated. If each of the 17,000 separator pores of 70nm diameter produces an equal amount of vapor, this would result in 0.213mg/s of total vapor production.

It is important to note that this method relies on wind velocity above each pore. Without more complex modeling techniques or experimentation, it is difficult to develop reasonable bounds for wind velocity for pool evaporation at this scale. Additionally, the nanoscale pore size may increase the relative influence of intermolecular forces on the flow of individual particles. These potential effects are not the focus of this study, but may need to be accounted for depending on experimental performance.

Evaporating gases were assumed to expand in the chamber as ideal gases, with contributions to chamber pressure from vapor generation expanding to fill a volume defined by Equation 9

$$P = \frac{m_E R_P T}{V} \tag{9}$$

where P is the pressure increase resulting from vapor generation. R_P, T, and m_E represent propellant specific gas constant, temperature, and evaporated mass into chamber volume V.

These pressure contributions were combined with expansion chamber ambient pressure and pressure losses due to gas evacuation through the nozzle to develop a time marching solution for chamber pressure. This pressure was then used as inlet pressure for the nozzle for thrust calculation.

NOZZLE PERFORMANCE

Nozzle Geometry

A suitable nozzle diameter was selected such that average mass flow rate would match the rate of vapor generation across the phase separator. Using the equation for mass flow rate given by Sutton and Biblarz [12].

$$\dot{m} = p_1 A_t \gamma \frac{\sqrt{\frac{2}{\gamma+1}^{\frac{\gamma+1}{\gamma-1}}}}{\sqrt{\gamma RT}} \tag{10}$$

where $\dot{m}$ is mass flow rate through the nozzle, p_1 is nozzle inlet pressure, A_t the nozzle throat area, γ the specific heats ratio, with gas constant R and temperature T. Assuming vapor flows through the nozzle without losses, the maximum operating exit plane Mach number may be determined according to Equation 11 given by Zucker [13]

$$T_t = T\left(1 + \frac{\gamma-1}{2} M^2\right) \tag{11}$$

where T_t is stagnation temperature and M is Mach number. By setting the temperatures to the propellant storage and freezing temperatures, the maximum allowable Mach number to prevent freezing inside the nozzle is retrieved. Given this Mach number, the ideal nozzle area ratio is determined using Equation 12

$$\epsilon = \frac{1}{M^2}\left[\frac{1+\frac{\gamma-1}{2}M^2}{\frac{\gamma+1}{2}}\right]^{\frac{\gamma+1}{2(\gamma-1)}} \tag{12}$$

Using a range of possible expansion ratios, corresponding exit temperatures were calculated and plotted relative to propellant freezing temperature. As shown below in Figure 5, an expansion ratio of 2.03 or lower would allow propellant vapors to exit the nozzle without freezing.

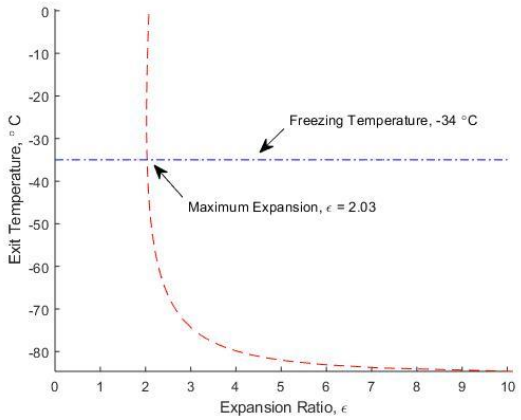

Figure 5. Possible expansion ratio relative to exit plane exhaust temperature

Thrust Performance

To determine if this system will produce sufficient thrust to counteract drag, thrust can be calculated using mass flow rate, $\dot{m}$, thrust coefficient, C_F, and characteristic velocity, c^*, via Equation 13

$$F = \dot{m} c^* C_F \tag{13}$$

where thrust coefficient and characteristic velocity are obtained as functions of pressure and specific heats ratios, γ, as given in Equations 14 and 15

$$C_F = \sqrt{\frac{2\gamma^2}{\gamma-1}\left(\frac{2}{\gamma+1}\right)^{\frac{\gamma+1}{\gamma-1}}\left[1 - \frac{p_2}{p_1}^{\frac{\gamma-1}{\gamma}}\right]} + \frac{p_2 - p_3}{p_1}\frac{A_2}{A_t} \tag{14}$$

$$c^* = \frac{\sqrt{\gamma RT}}{\gamma\sqrt{\frac{2}{\gamma+1}^{\frac{\gamma+1}{\gamma-1}}}} \tag{15}$$

According to the above equations applied through a time-marching simulation, steady state thrust of 158μN was determined. This thrust projection was then compared to drag forces acting on the spacecraft as a function of mean density at its orbital altitude. Atmospheric drag forces acting on the spacecraft were determined using circular speed for a 250km orbit, a drag coefficient of 2.2, and area normal to the satellite direction of motion. Atmospheric density was determined according to the 1976 NASA Standard Atmosphere [14] and values published by Wertz et al

[15]. These parameters were used as inputs to Equation 16

$$F_D = \frac{1}{2}\rho V^2 C_D A_{CS}(1 + 4\cos(45°)) \quad (16)$$

where C_D is the drag coefficient and A_{CS} is the cross-sectional area of a 1U CubeSat. By this method, a total atmospheric drag of 125μN was calculated. Since this method projects roughly 25% greater thrust production above the drag threshold, orbital altitude may increase throughout the duration of the mission. However, this excess thrust margin serves to compensate for losses not shown in ideal thrust modeling, such as off-velocity-vector-pointing, while ensuring that the steady state operating thrust does not fall below the value required to counteract drag. WISP specific impulse was calculated for a 100μm diameter nozzle using Equation 17. Using a thrust coefficient of 1.49 and characteristic velocity of 516 m/s, a specific impulse of 51s was calculated.

$$I_{sp} = \frac{c^* C_F}{g_0} \quad (17)$$

Runtime

For the time-marching simulation implemented in this study, thrust, mass flow, and vapor generation were calculated once per second until propellant was depleted. This simulation did not take into account variations in chamber temperature or misalignment between thrust vector and direction of motion due to spacecraft rotation. Further simulations will be conducted to determine spacecraft attitude effects with attitude stabilizers deployed as discussed by Bishop [1]. Thermal effect simulations will also be performed to bound minimum and maximum thrust performance based on temperature fluctuations for a typical orbit and spacecraft thermal properties.

With steady state thrust of sufficient strength to counteract drag determined, overall mission lifetime can be determined simply as a function of average mass flow rate and initial propellant reserves, m_0, using Equation 18.

$$t = \frac{\dot{m}}{m_0} \quad (18)$$

Applying this equation to steady state mass flow rate of 2.13mg/s and an initial propellant mass of 775g, a projected runtime of 42.13 days was determined. Steady state thrust and propellant reserve depletion due to vapor generation throughout the mission are depicted below in Figure 6. A constant thrust is a result of the phase separator and evaporation chamber setup where the relative throat area, thus the limitation on the flow rate, is much smaller than the evaporation chamber's ability to maintain pressure in the chamber. As the propellant is depleted, the evaporation chamber pressure decrease is minimal until the complete depletion of the propellant occurs.

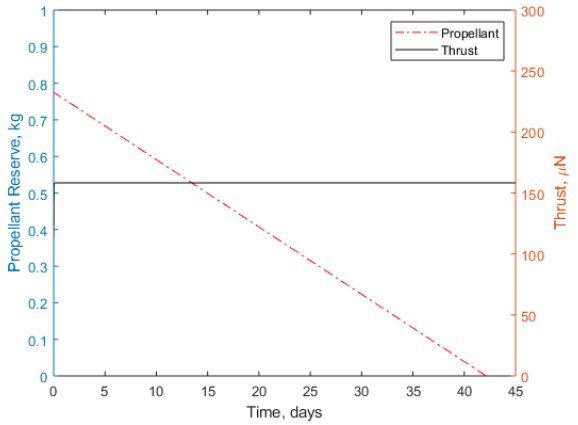

Figure 6. WISP thrust and propellant reserves throughout mission life

If this method can be experimentally validated, WISP may be capable of extending mission life by up to 40 days while occupying 1U of payload volume and drawing no electrical power at steady state. Such a capability would enable the rapid fielding of new sensing technologies without contributing to the growth of orbital debris.

EXPERIMENTAL VALIDAITON AND FUTURE WORK

Calculations discussed previously only serve as predictions of possible performance. Since all propellant properties were calculated according to curve fits of published data, experimental validation of these data should be performed. In order to measure evaporation rate directly, a simple thermal vacuum chamber has been constructed using a commercially available steel vacuum pot and refrigerator equipped with temperature and pressure gauges along with a scale. Viscosity data will be validated via Couette viscometry at various temperatures. By collecting these property data across multiple temperatures and pressures, similar polynomial fit functions may be developed and compared with results from functions obtained previously

This study does not address detumbling, attitude control, or deployment at altitudes other than 250km. Non-circular orbit geometry and spacecraft attitudes not aligned with the direction of motion were not considered. While previous models suggest that WISP's attitude stabilization hardware will limit off-axis oscillations to roughly 20°, oscillation-induced thrust vectoring cannot be ignored. Mission lifetime and pointing effects

resulting from these phenomena must be explored prior to actual implementation.

Thermal effects must also be accounted for to better simulate thrust performance in common spacecraft operating conditions including eclipse and direct sunlight. System performance may be improved by adding a battery-operated heater to the system independent of sensing payload electrical power systems. Since the expansion chamber generally offers more volume than is expressly required to generate thrust, placement of a larger battery within that volume to operate the nozzle actuation value, attitude stabilizer burn resistor and nozzle heater could be implemented.

Lastly, this study does not take into consideration the non-ideal molecular behavior including entropy, compressibility, and reaction temperature effects in evaporation determination and thrust calculation. Proper understanding of these phenomena is critical to thrust determination and must be better understood to ensure mission success.

CONCLUSION

A conceptual design for a passive phase separation cold gas thruster for nanosatellite applications has been developed. This system is capable of producing roughly 150μN of thrust, allowing it to overcome drag forces acting on a standard 3U CubeSat while drawing no electrical power. Initial projections indicated that this system, along with a passive attitude stabilization hardware that leverages air drag, should be capable of maintaining orbit for a 3U or smaller CubeSat for at least one month. By introducing orbit maintenance and attitude stabilization hardware in a modular, CubeSat-compatible form factor, WISP offers researchers the opportunity to field new sensors rapidly and with streamlined integration. Offering a low-cost, operationally-simple nanosatellite bus solution, WISP holds promise for greatly increasing capability of CubeSat-based science.

ACKNOWLEDGMENT

The authors would like to express sincere thanks to Professor Jeffrey Fitzgerald, Ph.D. of the United States Naval Academy Chemistry Department.

REFERENCES

1. Bishop, A. and Kang, J, “Analysis of Aerodynamic Stabilization and Drag Makeup Propulsion for Ultra-low Earth Orbit Spacecraft”, Joint 32nd International Symposium on Space Technology and Science and 9th Nano-Satellite Symposium, Fukui, Japan, June 17, 2019
2. Engineering ToolBox, (2018). *Methanol - Density and Specific Weight*. [online] Available at: https://www.engineeringtoolbox.com/methanol-density-specific-weight-temperature-pressure-d_2091.html.
3. Engineering ToolBox, (2018). *Methanol - Dynamic and Kinematic Viscosity*. [online] Available at: https://www.engineeringtoolbox.com/methanol-dynamic-kinematic-viscosity-temperature-pressure-d_2093.html.
4. Engineering ToolBox, (2003). *Water - Density, Specific Weight and Thermal Expansion Coefficient*. [online] Available at: https://www.engineeringtoolbox.com/water-density-specific-weight-d_595.html.
5. Engineering ToolBox, (2004). *Water - Dynamic and Kinematic Viscosity*. [online] Available at: https://www.engineeringtoolbox.com/water-dynamic-kinematic-viscosity-d_596.html.
6. Engineering ToolBox, (2018). *Methanol - Thermophysical Properties*. [online] Available at: https://www.engineeringtoolbox.com/methanol-methyl-alcohol-properties-CH3OH-d_2031.html
7. Derlacki, Z. J., Easteal, A. J., Edge, V. J., Woolf, L. A. & Roksandic, Z. *Diffusion Coefficients of Methanol and Water and the Mutual Diffusion Coefficient in Methanol-Water Solutions at 278 and 298 K*. Journal of Physical Chemistry, Volume 89. (1985). pp. 5318 5322.
8. Dortmund Data Bank, LLC. *Saturated Vapor Pressure: Calculation by Antoine Equation*. [online] Available at: http://ddbonline.ddbst.com/AntoineCalculation/AntoineCalculationCGI.exe?component=Methanol
9. Maxwell, James Clerk; Strutt, John William (1911). “Capillary Action”. In Chisholm, Hugh (ed.). *Encyclopædia Britannica*. 5 (11th ed.). Cambridge University Press. pp. 256–275.
10. Monika Souc˘kova´, Jaroslav Klomfar, and Jaroslav Pa´tek. *Measurement and Correlation of the Surface Tension-Temperature Relation for Methanol*. Journal of Chemical Engineering Data, Volume 53. (2008). pp. 2233-2236.
11. Bubbico, Roberto & Mazzarotta, Barbara. *Predicting Evaporation Rates from Pools.* Chemical Engineering Transactions, Volume 48. (2016). pp. 49-54.
12. Sutton, George P. & Biblarz, Oscar. *Rocket Propulsion Elements, Ninth Edition.* (2017). pp. 47-67, 749-750.

13. Zucker, Robert D. & Biblarz, Oscar. *Fundamentals of Gas Dynamics, Second Edition.* (2002). pp. 83-99.

14. National Aeronautics and Space Administration. *The 1976 Standard Atmosphere Above 86-km Altitude*. (1976). Edited by Minzer, R. A.

15. Wertz, James R., Everett, David F. & Puschell, Jeffrey J. *Space Mission Engineering: The New SMAD.* (2011).